Monthly Notices
of the
ROYAL ASTRONOMICAL SOCIETY

MNRAS **513,** 2285–2291 (2022)
Advance Access publication 2022 April 13

https://doi.org/10.1093/mnras/stac1027

Pulsating hydrogen-deficient white dwarfs and pre-white dwarfs observed with *TESS* – IV. Discovery of two new GW Vir stars: TIC 0403800675 and TIC 1989122424

Murat Uzundag [1,2★] Alejandro H. Córsico,[3,4] S. O. Kepler [5] Leandro G. Althaus,[3,4] Klaus Werner [6] Nicole Reindl[7] and Maja Vučković[1]

[1]*Instituto de Física y Astronomía, Universidad de Valparaíso, Gran Bretaña 1111, Playa Ancha, Valparaíso 2360102, Chile*
[2]*European Southern Observatory, Alonso de Cordova 3107, Santiago, Chile*
[3]*Grupo de Evolución Estelar y Pulsaciones. Facultad de Ciencias Astronómicas y Geofísicas, Universidad Nacional de La Plata, Paseo del Bosque s/n, 1900 Argentina*
[4]*IALP - CONICET*
[5]*Instituto de Física, Universidade Federal do Rio Grande do Sul, 91501-970 Porto-Alegre, RS, Brazil*
[6]*Institut für Astronomie und Astrophysik, Kepler Center for Astro and Particle Physics, Eberhard Karls Universität, Sand 1, D-72076 Tübingen, Germany*
[7]*Institute for Physics and Astronomy, University of Potsdam, Karl-Liebknecht-Str. 24/25, D-14476 Potsdam, Germany*

Accepted 2022 April 6. Received 2022 April 5; in original form 2022 February 4

ABSTRACT

We present two new GW Vir-type pulsating white dwarf stars, TIC 0403800675 (WD J115727.68-280349.64) and TIC 1989122424 (WD J211738.38-552801.18) discovered in the *Transiting Exoplanet Survey Satellite* (*TESS*) photometric data. For both stars, the *TESS* light curves reveal the presence of oscillations with periods in a narrow range between 400 and 410 s, which are associated with typical gravity (g)-modes. Follow-up ground-based spectroscopy shows that both stars have similar effective temperature ($T_{\rm eff} = 110\,000 \pm 10\,000$ K) and surface gravity ($\log g = 7.5 \pm 0.5$), but different He/C composition (mass fractions): He = 0.75 and C = 0.25 for TIC 0403800675, and He = 0.50 and C = 0.50 for TIC 1989122424. By performing a fit to their spectral energy distributions, we found for both stars radii and luminosities of $R = 0.019 \pm 0.002\,{\rm R}_{\odot}$ and $\log({\rm L}/{\rm L}_{\odot}) = 1.68^{+0.15}_{-0.24}$, respectively. By employing evolutionary tracks of PG 1159 stars, we find the masses of both stars to be $0.56 \pm 0.18\,{\rm M}_{\odot}$ from the $\log g$-$T_{\rm eff}$ diagram and $0.60^{+0.11}_{-0.09}\,{\rm M}_{\odot}$ from the Hertzsprung Russell diagram.

Key words: stars: evolution – stars: interiors – stars: oscillations (including pulsations) – white dwarfs.

1 INTRODUCTION

White dwarf (WD) stars are the end evolutionary state of all stars formed with initial masses below around 7−11 $\rm M_{\odot}$, which comprise more than 95 per cent of all stars in our Galaxy (Althaus et al. 2010). In the course of their evolution, WDs cross at least one phase of pulsational instability that converts them into pulsating variable stars. GW Vir variable stars are the hottest known class of pulsating WDs and pre-WDs, with 75 000 K $\leq T_{\rm eff} \leq$ 250 000 K and $5.3 \leq \log g \leq 8$ (Werner et al. 2021). They are located within a definite instability strip (see fig. 1 of Córsico et al. 2019). GW Vir stars include some objects that are still surrounded by a nebula, called the variable planetary nebula nuclei (PNNVs), and some objects that lack a nebula, which are called DOVs. Both groups (DOVs and PNNVs) are frequently referred to as GW Vir variable stars. GW Vir stars display brightness fluctuations with periods in the range 300–6000 s, and amplitudes up to a few mmag (1 mmag = 1 ppt), associated with low-order ($\ell \leq 2$) non-radial g(gravity) modes.

GW Vir stars are pulsating PG 1159 stars (after the prototype of the spectroscopic class, the star PG 1159−035), which are hydrogen(H)-deficient post-AGB stars with surface layers rich in helium (He), carbon (C), and oxygen (O) (Werner & Herwig 2006). It is believed that this mixture is a result of a mixing event produced by a late He flash during the so-called born-again episode (Fujimoto 1977; Schoenberner 1979; Iben et al. 1983; Althaus et al. 2010). PG 1159 stars are considered the evolutionary link between post-AGB stars and most of the H-deficient WDs, including DO and DB WDs (Herwig et al. 1999; Althaus et al. 2005; Sowicka et al. 2021). They can be either the outcome of single star evolution (late thermal pulse scenario, LTP, or very late thermal pulse scenario, VLTP) or binary star evolution (double WD merger). The classification of GW Vir stars includes also the pulsating Wolf-Rayet central stars of a planetary nebula ([WC]) and Early-[WC] = [WCE] stars since they share the same pulsation properties of pulsating PG 1159 stars (Quirion, Fontaine & Brassard 2007). Thus far about 50 PG 1159 stars have been identified (Werner et al. 2021). Amongst them, approximately 50 per cent (22 objects; see Córsico et al. 2019; Uzundag et al. 2021) have been discovered to be pulsating. It is especially important to find new pulsators of this class, as they can provide insight into the AGB and VLTP/LTP phases, as well as angular momentum loss throughout the extensive mass-loss phases (and references therein Kepler et al. 2014).

Prior to space missions, GW Vir stars were monitored through long-term observations carried out by the multisite photometric campaign with the 'Whole Earth Telescope' (WET; Nather et al.

★ E-mail: murat.uzundag@postgrado.uv.cl

Table 1. Log of spectroscopic observations.

TIC	Name	RA (J2000)	Dec (J2000)	G_{mag}	Obs. Date (UT)	Exp. (s)	Grating (l mm^{-1})	Resolution ($\Delta\lambda$ (Å))	S/N
0403800675	WD J115727.68−280349.64	11:57:28	−28:03:53	16.16	2021-06-18 03:26:17	1200	400	4.6	65
1989122424	WD J211738.38−552801.18	21:17:40	−55:28:16	16.75	2021-06-19 07:54:54	900	400	4.6	70

1990). These observations provided invaluable sources of information to constrain their internal structure (Winget et al. 1991). The spectral observations from the Sloan Digital Sky Survey (SDSS; York et al. 2000) promoted the discovery of a GW Vir pulsating star, SDSS J075415.12+085232.18 (Kepler et al. 2014). The advent of the *Kepler* space mission has resulted in important advances in the study of pulsating stars in general (Aerts 2021; Kurtz 2022) and pulsating WDs in particular (Córsico 2020). Unfortunately, during the main mission of the *Kepler* satellite (Borucki et al. 2010), no GW Vir star was observed. During the *Kepler* extended mission (*K2*; Howell et al. 2014), the prototype PG 1159−035 was observed during almost 50 d of coverage and the findings will be reported soon (G. O. da Rosa et al., in preparation). Currently, uninterrupted observations from space with the *Transiting Exoplanet Survey Satellite* (*TESS*) allow us to find and characterize new and already known GW Vir stars. Indeed, *TESS* has allowed a detailed asteroseismological analysis of a number of formerly known GW Vir stars (Córsico et al. 2021), enabling the determination of their fundamental parameters and evolutionary properties. The discovery of two new GW Vir stars has been presented by Uzundag et al. (2021). In these studies, using asteroseismic techniques (e.g. asymptotic period spacing and rotational splittings), the authors were able to determine the internal chemical stratification, total mass and, in some cases, rotation velocity of GW Vir stars.

In this work, we present the discovery of two new GW Vir stars, TIC 0403800675 (WD J115727.68-280349.6) and TIC 198912242 (WD J211738.38-552801.1), which were observed during the survey phase of the southern ecliptic hemisphere cycle 1 and 3 of *TESS*. In addition, for each target we obtained low-resolution spectra and fitted model atmospheres to estimate their fundamental atmospheric parameters, and examined the *TESS* light curve to identify the pulsational modes. This study is the fourth part of a series of papers devoted to the study of pulsating H-deficient WDs and pre-WDs observed with *TESS*. The first article was devoted to a set of six already known GW Vir stars including PNNVs and DOVs (Córsico et al. 2021), the second to the discovery of two new GW Vir stars of the DOV type (Uzundag et al. 2021), and the third to a detailed asteroseismological analysis of the prototype of the pulsating DB WD, GD 358 (Córsico et al. 2022).

The paper is organized as follows. In Section 2, we present the details of spectroscopic observations and the data reduction. In Section 3, we derive atmospheric parameters for each star by fitting synthetic spectra to the newly obtained low-resolution spectra. In Section 5, we analyse the photometric *TESS* data and give details on the frequency analysis. Finally, in Section 6, we summarize our main results.

2 SPECTROSCOPY

TIC 0403800675 (WD J115727.68−280349.6) and TIC 198912242 (WD J211738.38−552801.1) were classified as WD candidates by Gentile Fusillo et al. (2019) from their colours and *Gaia* DR2 parallax. The *Gaia* DR3 parallax and corresponding distance for TIC 0403800675 are $\pi = 1.86^{+0.07}_{-0.06}$ mas and $d = 535.41^{+19.49}_{-18.44}$ pc, while for TIC 198912242 are $\pi = 1.45^{+0.05}_{-0.06}$ mas and $d = 688.27^{+22.34}_{-26.31}$ pc (Bailer-Jones et al. 2021), respectively.

To estimate the atmospheric parameters of TIC 0403800675 and TIC 1989122424, we obtained spectra with the Goodman High-Throughput Spectrograph (GHTS; Clemens, Crain & Anderson 2004) at the SOAR 4.1-m telescope on Cerro Pachón. We reduced the spectroscopic data using the instrument pipeline[1] including overscan, trim, slit trim, bias, and flat corrections. We employed a method developed by Pych (2004), which is included in the pipeline, to identify and remove cosmic rays. After the reduction was completed, the wavelength calibration has been applied by using pyraf[2] (Science Software Branch at STScI 2012). We used the frames produced with the internal He-Ar-Ne comparison lamp at the same telescope position as the targets in order to apply wavelength calibrations. The sixth order Legendre function is used to calibrate the pixel-wavelength correspondence using an atlas of known He-Ar-Ne lines. Finally, we used the standard star Feige 110 seen with the identical apparatus to normalize the spectra with a high-order Legendre function. Table 1 contains the details of the spectroscopic observations, including the name of the targets, right ascension, declination, Gaia magnitude, date, exposure time, grating, resolution, and S/N ratio.

3 SPECTRAL FITTING

The spectral lines in the spectra of TIC 0403800675 and TIC 1989122424 are all from He II and C IV. Oxygen, which is the most abundant element in PG 1159 stars after He and C, and nitrogen (N) – which is present as a trace element in some PG 1159 stars – may be visible in spectra with higher resolution and signal-to-noise ratio. In the spectra of both stars, there are no indications of the presence of H.

For the spectral analysis, we used a grid of line-blanketed non-local thermodynamic equilibrium (non-LTE) model atmospheres consisting of H, He, and C as introduced by Werner, Rauch & Kepler (2014). The grid spans $T_{\rm eff}$ = 60 000–140 000 K in effective temperature and $\log g$ = 4.8–8.3 in surface gravity, with steps of 5000 K or 10 000 K and 0.3 dex, respectively. C/He mass ratios in the range 0.0–1.0 were considered, namely C/He = 0.0, 0.03, 0.09, 0.33, 0.77, and 1.0. The hydrogen abundance was set to zero. Synthetic spectra were convolved with a Gaussian accounting for the spectral resolution of the observations. The best-fitting models were chosen by visual comparison with the rectified observed spectra.

The model fits are depicted in Fig. 1. Both stars have $T_{\rm eff} = 110\,000 \pm 10\,000$ K and $\log g = 7.5 \pm 0.5$, but a different atmospheric composition. For TIC 0403800675, we found He $= 0.75^{+0.05}_{-0.15}$ and C $= 0.25^{+0.15}_{-0.05}$ and for TIC 1989122424, we measured He $= 0.50^{+0.20}_{-0.05}$ and C $= 0.50^{+0.05}_{-0.20}$ (mass fractions). An upper limit to the abundance of hydrogen was determined to be 5 per cent by mass. At

[1] https://github.com/soar-telescope/goodman_pipeline
[2] http://www.stsci.edu/institute/software_hardware/pyraf

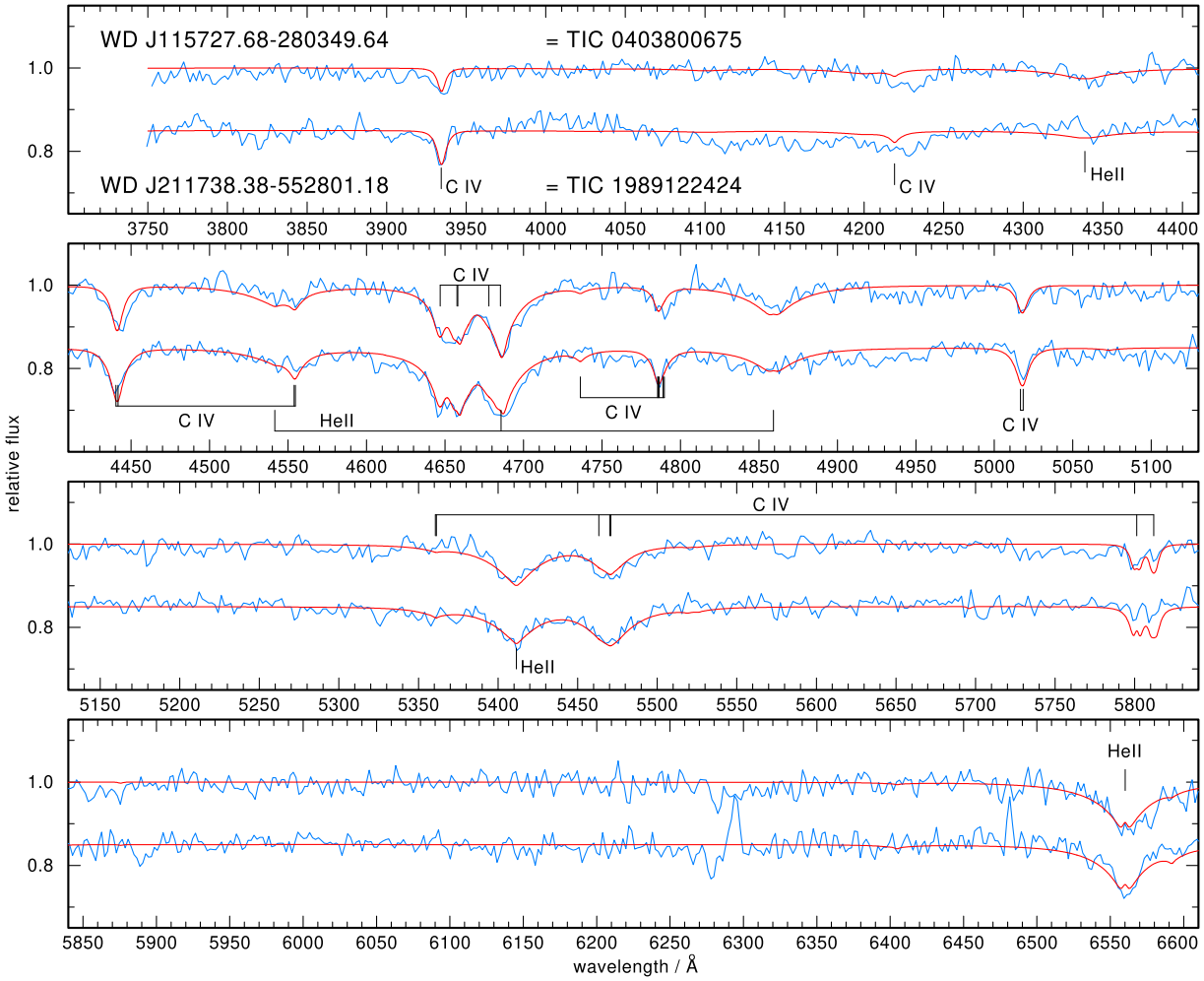

Figure 1. Optical spectra of the two new GW Vir stars (blue graphs) obtained with SOAR/Goodman. Overplotted are the best-fitting models (red). Identifications of He II and C IV lines are marked.

this abundance, a H α emission core would be detectable and the H β line blend with the respective He II line would be too strong.

In Fig. 2 we show the location of the new GW Vir stars in the log g-$T_{\rm eff}$ diagram. By linear interpolation among the PG 1159 evolutionary tracks of Althaus et al. (2005) and Miller Bertolami & Althaus (2006), we derive a stellar mass of $M_\star = 0.56 \pm 0.18 M_\odot$ for TIC 0403800675 and TIC 1989122424. These evolutionary tracks of PG 1159 stars have been compared by Miller Bertolami & Althaus (2007) with other independent published calculations. These authors concluded that the differences in the inferred masses using different sets of PG1159 evolutionary tracks must be less than ~ 0.01 M$_\odot$. This constitutes the systematic errors associated with the Althaus et al. (2005) and Miller Bertolami & Althaus (2006) evolutionary tracks. We conclude that the errors in the spectroscopic mass of the two new GW Vir stars come mainly from the uncertainties in the spectroscopic log g and $T_{\rm eff}$.

4 SED FITTING

In order to determine the radii of the two stars, we performed a fit to the spectral energy distribution (SED), by varying the solid angle $\pi (R/d)^2$, (which relates the flux at the surface of the system to what is received at Earth) until a good agreement of the predicted fluxes and the observations was found as shown in Fig. 4. We employed our best-fitting model atmospheres for both stars, and using the Fitzpatrick (1999) reddening law, our predicted spectra were reddened for different values of $E_{\rm B\text{-}V}$. We used the distance provided by Bailer-Jones et al. (2021) and employed photometry from *GALEX* (Bianchi, Conti & Shiao 2014), *Gaia* DR2 and eDR3 (Gaia Collaboration 2021), and Pan-STARRS1 (Chambers et al. 2016). Magnitudes were converted into fluxes using the VizieR Photometry viewer.[3] For TIC 0403800675, we find a reddening of $E_{\rm B\text{-}V} = 0.034$ mag and for TIC 1989122424 we find $E_{\rm B\text{-}V} = 0.048$ mag. Both values are in agreement with the upper limits of the 2D dust map provided by Schlafly & Finkbeiner (2011). For both stars we determine a radius of $R = 0.019 \pm 0.002\,{\rm R}_\odot$. Using $L = 4\pi\,\sigma\,R^2 T_{\rm eff}^4$, where σ is the Stefan-Boltzmann constant, we calculate for both stars a luminosity of $\log({\rm L/L}_\odot) = 1.68^{+0.15}_{-0.24}$. This allows us now to also derive the masses for TIC 0403800675 and TIC 1989122424 in the Hertzsprung–Russell diagram (HRD, see Fig. 4). By linear interpolation among the PG 1159 evolutionary tracks of Miller Bertolami & Althaus (2006), we derive a stellar mass of $M_\star = 0.60^{+0.11}_{-0.09} M_\odot$ for both stars, which is in agreement with the masses derived from the log g–$T_{\rm eff}$ diagram (see Fig. 3). The main characteristics of TIC 0403800675 and TIC 1989122424 are listed in Table 2 including atmospheric parameters, masses, luminosities, radii, distances, and reddening.

[3] http://vizier.unistra.fr/vizier/sed/

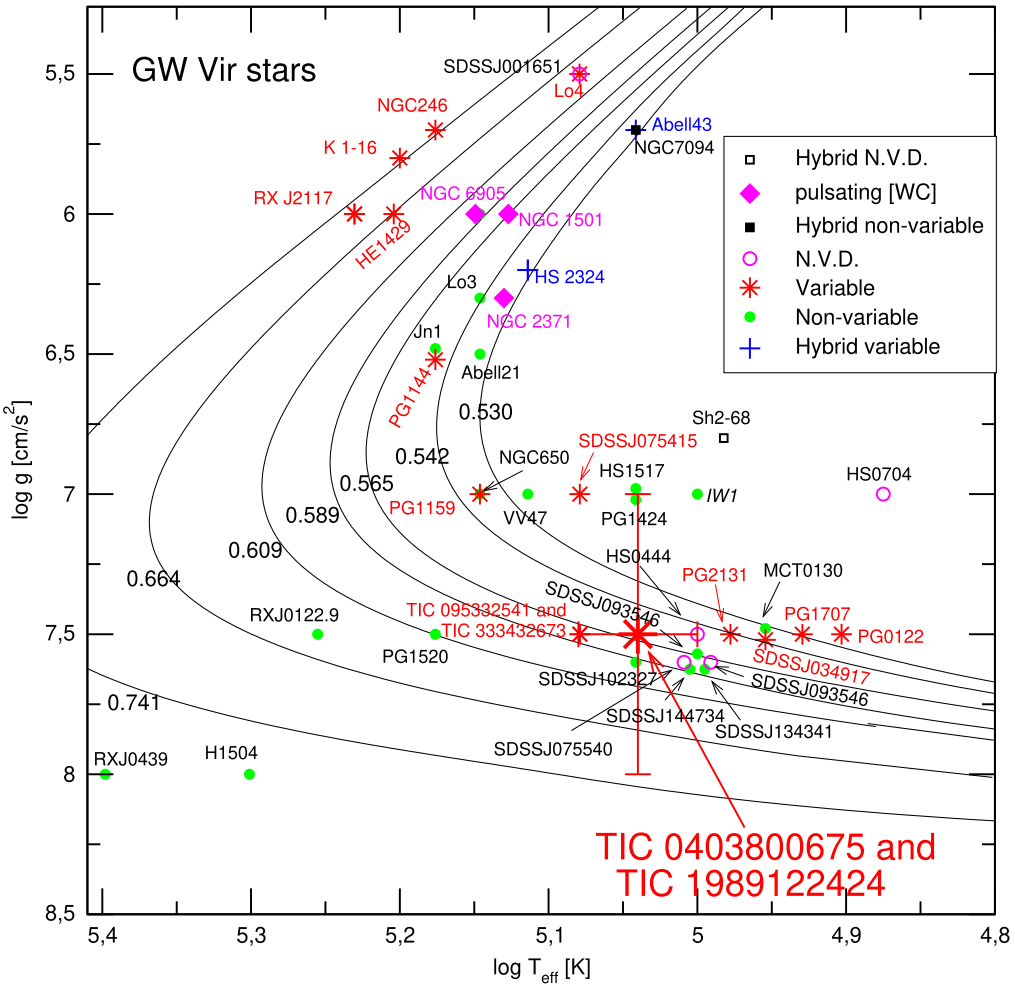

Figure 2. The already known variable and non-variable PG 1159 stars and variable [WCE] stars in the $\log T_{\rm eff} - \log g$ diagram. Thin solid black curves show the post−born again evolutionary tracks from Althaus et al. (2005) and Miller Bertolami & Althaus (2006) for different stellar masses noted on top of each track. 'N.V.D.' stands for PG 1159 stars with no variability data. 'Hybrid' refers to PG 1159 stars exhibiting H in their atmospheres. The location of the two new GW Vir stars TIC 0403800675 and TIC 1989122424 is emphasized with a large red star symbol and error bars. Both stars share the same spectroscopic surface parameters, $T_{\rm eff} = 110\,000 \pm 10\,000$ K and $\log g = 7.5 \pm 0.5$.

5 PHOTOMETRIC OBSERVATIONS – *TESS*

TIC 0403800675 was observed by TESS in sector 10 between 2019 March 26 and April 22 and in sector 36 between 2021 March 7 and April 2. TIC 1989122424 was observed in a single sector 27 between 2020 July 4 and July 30 with only 120 s cadence.

The light curves were downloaded from The Mikulski Archive for Space Telescopes, which is hosted by the Space Telescope Science Institute (STScI)[4] as FITS format. The light curves were processed by the Science Processing Operations Center (SPOC) pipeline (Jenkins et al. 2016). We first downloaded the target pixel file (TPF) of interest from the MAST archive, which is maintained by the Lightkurve Collaboration (Lightkurve Collaboration 2018). The TPFs comprises an 11×11 postage stamp of pixels from the one of four CCDs per camera that the target is located on. The TPFs are examined to determine the amount of crowding and other potential bright sources near the target. Because both targets had a modest amount of crowding which we evaluated using the *CROWDSAP* parameter, that was set to 0.6 for TIC 1989122424 and 0.8 for TIC 0403800675. Therefore we have decided to use the pipeline aperture as it gave the most optimal result with respect to signal-to-noise ratio. We extracted times in barycentric corrected dynamical Julian days and fluxes (PDCSAP FLUX) from the FITS files. We converted the fluxes to fractional variations from the mean and transformed to amplitudes in parts-per-thousand (ppt). Finally, the data were sigma-clipped based on 5σ to remove the outliers which appear above five times the median of intensities. The resulting short-cadence (SC) light curve of TIC 040380067 comprises 29 298 images spanning 47.4 d, while the resulting SC light curve of TIC 1989122424 includes 16 478 data points spanning 23.9 d. TIC 0403800675 was also observed with ultra-short-cadence (USC) during 23.9 d in sector 36 that yield 93 122 images.

[4] http://archive.stsci.edu/

5.1 Frequency solution

The Fourier transform (FT) was used to examine the periodicities present in the light curves. The frequencies, amplitudes, and errors were estimated using both the *Period*04 and our custom tool. We fitted each frequency that appears above the 0.1 per cent false alarm probability (FAP). The FAP level was calculated by reshuffling the

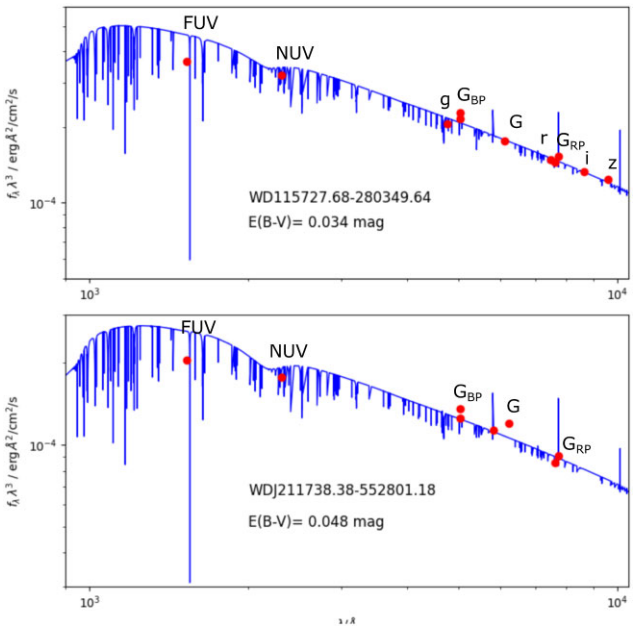

Figure 3. Fit to the SEDs of TIC 0403800675 (WD J115727.68-280349.64, upper panel) and TIC 1989122424 (WD J211738.38-552801.18, bottom panel). The red dots indicate filter-averaged fluxes that were converted from observed magnitudes. Error bars are smaller than symbol size. The blue solid lines represent our best-fitting model fluxes with the parameters as stated in Section 4. The assumed values for the interstellar reddening in each fit are indicated.

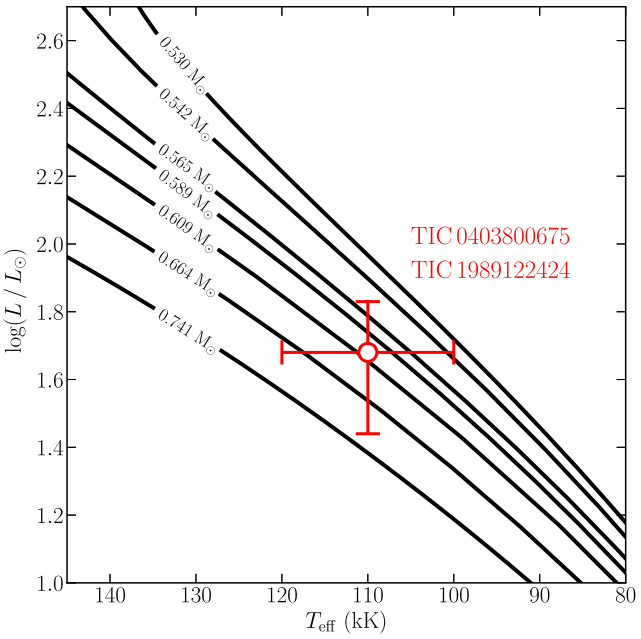

Figure 4. The location of the two new GW Vir stars TIC 0403800675 and TIC 1989122424 (emphasized with a large red dot symbol and error bars) in the HRD. The black curves show the post−born again evolutionary tracks from Miller Bertolami & Althaus (2006) for different stellar masses. Both stars share the same effective temperatures ($T_{\rm eff} = 110\,000 \pm 10\,000$ K) and luminosities ($\log(L_\star/L_\odot) = 1.68^{+0.15}_{-0.24}$).

Table 2. Properties of GW Vir pulsating stars studied in this work.

Quantity	TIC 0403800675	TIC 1989122424
$T_{\rm eff}$ (kK)	110 ± 10	110 ± 10
$M_\star$ ($M_\odot$)	0.56 ± 0.18	0.56 ± 0.18
$\log g$ (cm s^{-2})	7.5 ± 0.5	7.5 ± 0.5
(He, C)	$0.75^{+0.05}_{-0.15}$, $0.25^{+0.15}_{-0.05}$	$0.50^{+0.20}_{-0.05}$, $0.50^{+0.05}_{-0.20}$
$R_\star$ [$R_\odot$]	0.019 ± 0.002	0.019 ± 0.002
$\log(L_\star/L_\odot)$	$1.68^{+0.15}_{-0.24}$	$1.68^{+0.15}_{-0.24}$
$E(B-V)$ (mag)	0.034	0.048
π (mas)	$1.86^{+0.07}_{-0.06}$	$1.45^{+0.05}_{-0.06}$
d (pc)	$535.41^{+19.49}_{-18.44}$	$688.27^{+22.34}_{-26.31}$

light curves 1000 times as described in Kepler (1993). The errors of each frequency and amplitude of the pulsation modes were estimated using Monte Carlo simulations (Lenz & Breger 2005). Furthermore, we have calculated sliding Fourier transform (sFT) for both stars in order to see the temporal evolution of the pulsational modes over the course of *TESS* observations. To do so, we use a 9-d sliding window with a 2-d step size. A colour-scale in ppt units is used to depict the amplitudes. Following that, we calculate the Fourier transform of each subset and trail them in time.

For TIC 0403800675, we analysed *TESS* observations using the SC and USC modes. The SC mode samples every 2-min allowing us to analyse the frequency range up to the Nyquist frequency at about 4167 μHz, while the USC mode samples every 20-s permitting us to examine the frequency range up to the Nyquist frequency at about 25 000 μHz. For TIC 0403800675, we detected two significant frequencies at 2445 and 2450 μHz. In Fig. 5, we show FT of combined SC data of sector 10 and 36 (black lines) (top panel), while the middle panel, we present USC data of sector 36. The magenta lines show the FT of the pre-whitened light curves. The signals are 20 per cent more amplified in USC data. Sliding Fourier transform display the both identified peaks in Fig. 5. The frequencies detected for TIC 0403800675 are presented in Table 3.

For TIC 1989122424, we also detected two clear signals at similar region between 2450 and 2490 μHz using solely SC observations. In Fig. 6, we focus on this region and show the FT of the original light curve (black line) and the FT of the pre-whitened light curves (magenta line). In sFT, these peaks are also clearly visible along with some other peaks. The two reported peaks at 2466 and 2479 μHz are clearly visible in sFT and they are stable during the run. We also see that there is a peak at 2470 μHz, which is stable during the first 10 d. For this peak, we did not produce an non-linear least square (NLLS) fit to extract from the light curve. We need additional observations to confirm whether it is real pulsational peak or not. The detected frequencies for TIC 0403800675 are reported in Table 4.

We hypothesized that the two closely spaced frequencies in both amplitude spectra and sFT can be due to stellar rotation in which the pulsation frequencies are split into $2\ell + 1$ azimuthal components. Assuming these frequencies are dipole modes and result from stellar rotation, then the rotation periods would range from 1.02 to 2.04 d (depending on the missing azimuthal order) for TIC 0403800675 and 0.43 d to 0.87 d for TIC 1989122424. Given the rotation periods of the GW Vir pulsating stars, which range from 5 h to a few days (Córsico et al. 2019, 2021), any of the potential solutions that we estimate for TIC 0403800675 and TIC 1989122424 could be conceivable. Furthermore, we note that the rotational periods of GW Vir stars cover about the same period range as white dwarfs showing ultra-highly excited (UHE) metals in their optical spectra. Reindl et al. (2021) discovered recently that this latter class of

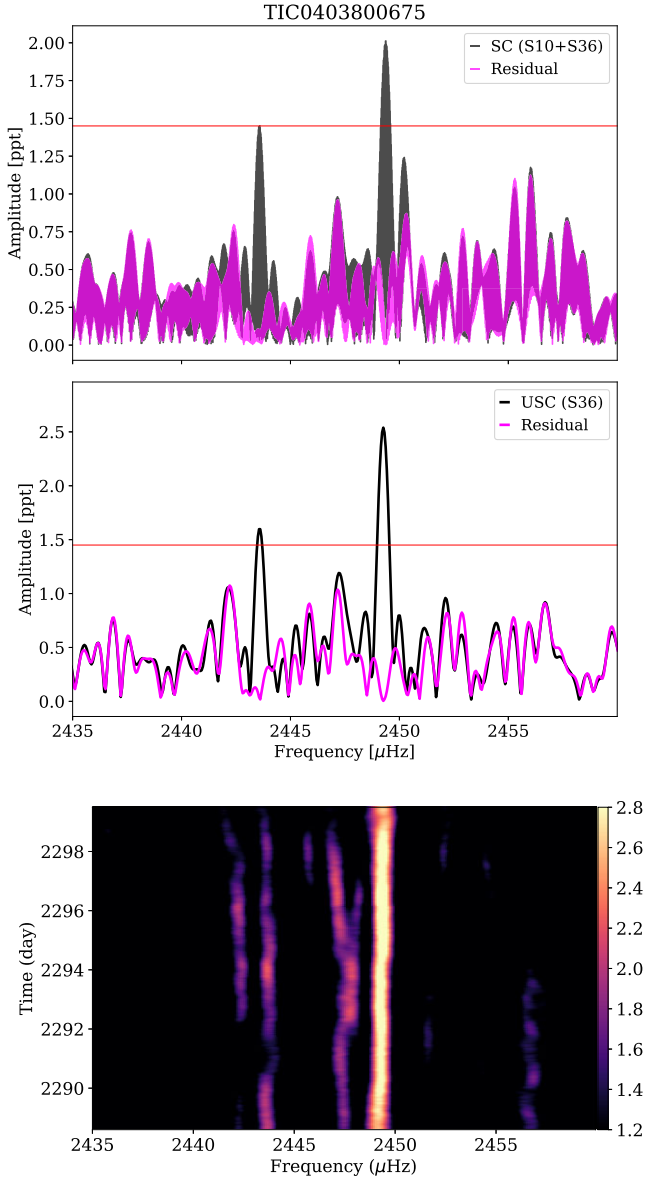

Figure 5. Top: Fourier transform of short-cadence data of sector 10 and 36 (black lines) for TIC 0403800675. The magenta line depicts the FT of the pre-whitened light curve. The horizontal red line indicates the 0.1 per cent FAP level. Middle: Fourier transform of ultra-short-cadence data of sector 36 (black lines) for TIC 0403800675. The red and magenta lines are the same as top panel the 0.1 per cent FAP level and the FT of the pre-whitened light curve, respectively. Bottom: Sliding Fourier transform of ultra-short-cadence data of sector 36 data of TIC 0403800675. The colour-scale illustrates amplitude in parts-per-thousand.

Table 3. Identified frequencies, periods, and amplitudes (and their uncertainties) and the signal-to-noise ratio in the data of TIC 0403800675. Frequency and amplitude that are detected in both sector 10 and 36.

Peak	ν (μHz)	Π (s)	A (ppt)	S/N
f_1	2443.597(51)	409.232(86)	1.63(33)	4.3
f_2	2449.261(33)	408.286(55)	2.54(33)	6.3

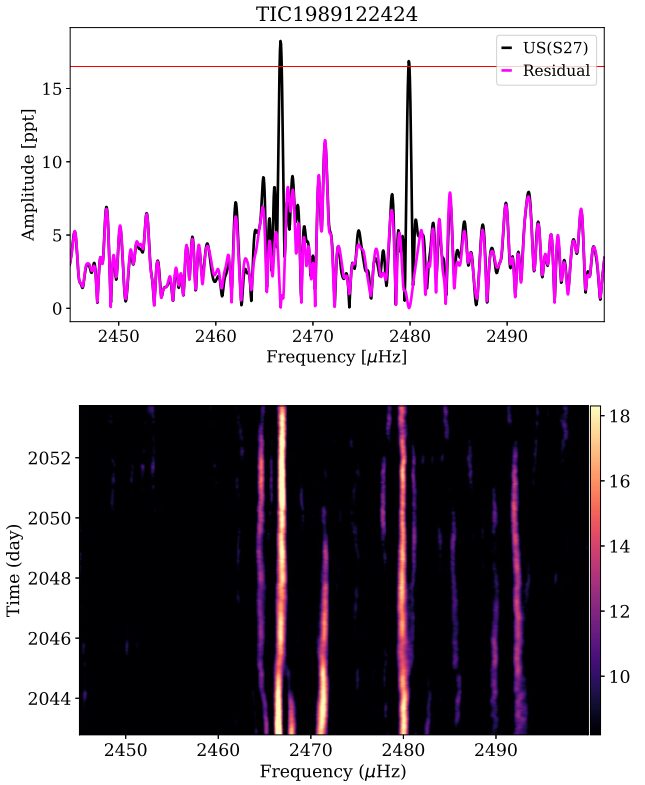

Figure 6. Top: Fourier transform of short-cadence data of sector 27 of TIC 1989122424. The horizontal red line indicates the 0.1 per cent FAP level. The magenta line depicts the FT of the pre-whitened light curve. Bottom: Sliding Fourier transform of the same data-set of TIC 1989122424. The colour-scale illustrates amplitude in parts-per-thousand.

Table 4. Identified frequencies, periods, and amplitudes (and their uncertainties) and the signal-to-noise ratio in the data of TIC 1989122424.

Peak	ν (μHz)	Π (s)	A (ppt)	S/N
f_1	2466.673(41)	405.404(68)	18.35(2.89)	5.1
f_2	2479.888(44)	403.243(72)	16.99(2.89)	4.7

white dwarfs show photometric periods between 6 h to 3 d and that their variability is likely caused by spots on the surfaces of these stars and/or geometrical effects of circumstellar material (see also Reindl et al. 2019). Since UHE white dwarfs are considered to be in an evolutionary stage immediately following that of the GW Vir pulsators, it would be interesting to know the rotational periods of more GW Vir stars in order to test a possible evolutionary connection.

6 CONCLUSIONS

In this paper, we have presented the discovery of two new GW Vir pulsating white dwarfs TIC 0403800675 and TIC 1989122424. We derived atmospheric parameters for TIC 0403800675 and TIC 1989122424 by fitting synthetic spectra to the newly obtained low-resolution SOAR/GOODMAN spectra. The determined spectroscopic parameters demonstrate that TIC 0403800675 and TIC 1989122424 are the same to within errors in terms of surface temperature and surface gravity ($T_{\rm eff} = 110\,000 \pm 10\,000$ K and $\log g = 7.5 \pm 0.5$) and they are only different regarding the surface C and He abundance. By performing a fit to the SEDs and parallaxes we

found for both stars radii and luminosities of $R_\star = 0.019 \pm 0.002\,R_\odot$ and $\log(L_\star/L_\odot) = 1.68^{+0.15}_{-0.24}$, respectively. Using the Althaus et al. (2005) and Miller Bertolami & Althaus (2006) evolutionary tracks of PG 1159 stars, we find a stellar mass for both stars of $0.56 \pm 0.18\,M_\odot$ from the log g-$T_{\rm eff}$ diagram and $0.60^{+0.11}_{-0.09}\,M_\odot$ from the HRD.

We have used the *TESS* 120-s data for both objects, while we made use of 20-s cadence data for only TIC 0403800675. Both stars exhibit just two periodicities in their amplitude spectra preventing us to make use of the seismic tools of rotational multiplets and asymptotic period spacing. Both pulsational frequencies that we extracted from the light curves are of the order of 7 min, attributable to non-radial pulsation g-modes. We also produced sFTs to see if the pulsation modes are resolved and stable throughout the *TESS* observations, which is limited to a single sector. The analysed data demonstrate that the main pulsational frequencies of our targets are stable and there is no clear pattern for rotational multiplets. Unfortunately, the presence of only two oscillation frequencies in the power spectrum of each star prevents us from making an asteroseismic modelling of these objects. We hope that more periods can be detected in the future, so that we can investigate the internal structure and evolutionary state of these stars through asteroseismological tools.

GW Vir stars evolve quickly, resulting in a significant period change due to cooling and contraction, which should be detected in a few years. As a result, these stars can be checked at least once a year to determine evolutionary changes as described by Costa & Kepler (2008).

ACKNOWLEDGEMENTS

We would like to thank the anonymous referee for the insightful comments and suggestions. MU thanks CONICYT Doctorado Nacional for financial support in the form of grant number 21190886 and the ESO studentship program. MU thanks Aleksandar Cikota for valuable discussions. Based on observations performed at the Southern Astrophysical Research (SOAR) telescope as part of the Chilean Time Allocation Committee (CNTAC) program numbers CN2020A-87, CN2020B-74, and CN2021A-52. This research uses data from the *TESS* mission, which was received from the Space Telescope Science Institute's MAST data archive. The NASA Explorer Program provides funding for the *TESS* program. This work has made use of data from the European Space Agency (ESA) mission Gaia (https://www.cosmos.esa.int/gaia), processed by the Gaia Data Processing and Analysis Consortium (DPAC, https://www.cosmos.esa.int/web/gaia/dpac/consortium). Funding for the DPAC has been provided by national institutions, in particular the institutions participating in the Gaia Multilateral Agreement. Part of this work was supported by AGENCIA through the Programa de Modernización Tecnológica BID 1728/OC-AR,and by the PIP 112-200801-00940 grant from CONICET. This research has made use of NASA's Astrophysics Data System Bibliographic Services, and the SIMBAD data base, operated at CDS, Strasbourg, France.

DATA AVAILABILITY

Data from *TESS* is available at the MAST archive https://mast.stsci.edu/search/hst/ui//. Ground based data will be shared on reasonable request to the corresponding author.

REFERENCES

Aerts C., 2021, Rev. Mod. Phys., 93, 015001
Althaus L. G., Serenelli A. M., Panei J. A., Córsico A. H., García-Berro E., Scóccola C. G., 2005, A&A, 435, 631
Althaus L. G., Córsico A. H., Isern J., García-Berro E., 2010, A&AR, 18, 471
Bailer-Jones C. A. L., Rybizki J., Fouesneau M., Demleitner M., Andrae R., 2021, VizieR Online Data Catalog, I/352
Bianchi L., Conti A., Shiao B., 2014, VizieR Online Data Catalog, 2335, 0
Borucki W. J. et al., 2010, Science, 327, 977
Chambers K. C. et al., 2016, preprint (arXiv:1612.05560)
Clemens J. C., Crain J. A., Anderson R., 2004, in Moorwood A. F. M., Iye M., eds, Proc. SPIE Conf. Ser. Vol. 5492, Ground-based Instrumentation for Astronomy. SPIE, Bellingham, p. 331
Córsico A. H., 2020, Front. Astron. Space Sci., 7, 47
Córsico A. H., Althaus L. G., Miller Bertolami M. M., Kepler S. O., 2019, A&AR, 27, 7
Córsico A. H. et al., 2021, A&A, 645, A117
Córsico A. H. et al., 2022, A&A, 659, A30
Costa J. E. S., Kepler S. O., 2008, A&A, 489, 1225
Fitzpatrick E. L., 1999, PASP, 111, 63
Fujimoto M. Y., 1977, PASJ, 29, 331
Gaia Collaboration 2021, A&A, 650, C3
Gentile Fusillo N. P. et al., 2019, MNRAS, 482, 4570
Herwig F., Blöcker T., Langer N., Driebe T., 1999, A&A, 349, L5
Howell S. B. et al., 2014, PASP, 126, 398
Iben I. J., Kaler J. B., Truran J. W., Renzini A., 1983, ApJ, 264, 605
Jenkins J. M. et al., 2016, in Chiozzi G., Guzman J. C., eds, Software and Cyberinfrastructure for Astronomy IV. SPIE, Bellingham, p. 99133E
Kepler S. O., 1993, Baltic Astron., 2, 515
Kepler S. O., Fraga L., Winget D. E., Bell K., Córsico A. H., Werner K., 2014, MNRAS, 442, 2278
Kurtz D., 2022, preprint (arXiv:2201.11629)
Lenz P., Breger M., 2005, Commun. Asteroseismol., 146, 53
Lightkurve Collaboration 2018, Lightkurve: Kepler and TESS time series analysis in Python, record ascl:1812.013
Miller Bertolami M. M., Althaus L. G., 2006, A&A, 454, 845
Miller Bertolami M. M., Althaus L. G., 2007, A&A, 470, 675
Nather R. E., Winget D. E., Clemens J. C., Hansen C. J., Hine B. P., 1990, ApJ, 361, 309
Pych W., 2004, PASP, 116, 148
Quirion P. O., Fontaine G., Brassard P., 2007, ApJS, 171, 219
Reindl N. et al., 2019, MNRAS, 482, L93
Reindl N., Schaffenroth V., Filiz S., Geier S., Pelisoli I., Kepler S. O., 2021, A&A, 647, A184
Schlafly E. F., Finkbeiner D. P., 2011, ApJ, 737, 103
Schoenberner D., 1979, A&A, 79, 108
Science Software Branch at STScI, 2012, PyRAF: Python alternative for IRAF, record ascl: 1207.011
Sowicka P., Handler G., Jones D., van Wyk F., 2021, ApJ, 918, L1
Uzundag M. et al., 2021, A&A, 655, A27
Werner K., Herwig F., 2006, PASP, 118, 183
Werner K., Rauch T., Kepler S. O., 2014, A&A, 564, A53
Werner K., Reindl N., Dorsch M., Geier S., Munari U., Raddi R., 2021, preprint (arXiv:2111.13549)
Winget D. E. et al., 1991, ApJ, 378, 326
York D. G. et al., 2000, AJ, 120, 1579

This paper has been typeset from a TEX/LATEX file prepared by the author.